

# BEAM TRACKING SIMULATIONS FOR STAGE 1 OF THE LASER-HYBRID ACCELERATOR FOR RADIOBIOLOGICAL APPLICATIONS (LhARA)

H. T. Lau\*, Department of Physics, Imperial College London, London, UK  
on behalf of the LhARA collaboration

## Abstract

The Laser-hybrid Accelerator for Radiobiological Applications (LhARA) is a unique and flexible facility proposed for radiobiological studies. The first stage of LhARA consists of an intense laser source interacting with a thin foil target producing a large flux of protons with energies up to 15 MeV. Particles will propagate through a combination of plasma (Gabor) lenses and magnetic elements to an achromat arc delivering the beam vertically to an *in-vitro* end station. An end-to-end simulation from the laser source to the end station is required to verify the conceptual design of the beamline. The laser-plasma interaction is simulated with Smilei (a particle-in-cell code) to produce a two-dimensional (2D) distribution of particles. Whilst it is possible to simulate the laser-plasma interaction in three dimensions (3D), access to the computing resources needed to run highly resolved simulations was not available. A sampling routine will be described which samples the 2D distribution to generate a 3D beam. The Monte Carlo simulation programs BDSIM and GPT were used to track the beam. Results of the simulations will be shown and compared to the results of an idealised Gaussian beam.

## INTRODUCTION

The Laser-hybrid Accelerator for Radiobiological Applications (LhARA) [1] is proposed as a novel and flexible facility for radiobiological research. A high power pulsed laser will drive the production of a large flux of protons and light ions. Gabor (plasma) lenses are used to capture and focus the divergent beam. It is expected that proton energies up to 15 MeV can be achieved. Further acceleration with a fixed-field alternating-gradient accelerator (FFA) is used to attain proton energies up to 127 MeV. The laser-hybrid approach allows for different energy regimes to be investigated using various ion species at instantaneous dose rates up to and beyond the “FLASH” regime [1, 2]. LhARA can be developed in two stages. Stage 1 involves the delivery of proton beams with energies between 12 MeV and 15 MeV to the low-energy *in vitro* end station, a schematic diagram can be seen in Fig. 1. Stage 2 includes the FFA and the delivery of multiple ion species to either an *in vitro* or *in vivo* end station.

## LASER SOURCE

A laser-driven source allows protons and ions to be captured at energies above those in conventional facilities, thereby evading the space-charge limitations on the instan-

\* h.lau17@imperial.ac.uk

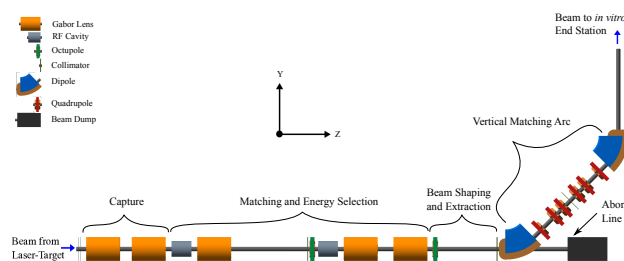


Figure 1: A schematic diagram of the beamline elements of Stage 1 of LhARA. It includes the laser-target and vacuum nozzle, the capture section, matching and energy selection, beam shaping, and the vertical arc to the end station.

taneous dose that can be delivered using conventional ion sources. Although some radiobiological studies have been conducted with a laser-driven source [3–5], these experiments were conducted at laser facilities with shifting priorities. LhARA positions itself to provide a dedicated ion beam for radiobiological research.

LhARA will operate in a laser-driven sheath-acceleration regime to produce a flux of protons and ions. Multi-MeV proton energies with beam qualities were first observed separately by three groups: Clark *et al.* [6], Maksimchuk *et al.* [7], and Snavely *et al.* [8]. The term “target normal sheath acceleration” (TNSA) mechanism was coined by Wilks *et al.* [9] when modelling the mechanism. The TNSA mechanism occurs when an intense and short laser pulse is focused onto a target. The electric field generated accelerates electrons near the surface of the target. These electrons are driven into the material, ionising the material. The electrons which penetrate through the target to the rear surface create a strong space-charge field or ‘sheath’. This sheath field accelerates contaminant ions on the surface of the target, producing a flux of ions. LhARA aims to use a commercially available laser system capable of delivering a significant proton flux at 15 MeV. A summary of the laser parameters for the laser source are presented in Table 1, a more comprehensive list of design parameters can be found in [2].

The energy spectrum of protons and ions produced from laser-driven beams exhibit a characteristic sharp cut off at the maximum energy. LhARA scales back from the maximum energy endpoint to focus on beam stability, allowing for reproducible measurements. A tape drive target based on a system developed at Imperial College London will be used, but diagnostics will need to be developed in order to measure the energy spectrum and spatial profile of the beam.

Table 1: Summary of Expected Laser Parameters for the Laser Source

Parameter	Value	Units
Laser power	100	TW
Laser energy	2.5	J
Pulse length	25	fs
Rep. rate	10	Hz
Focal spot size	3	$\mu\text{m}$
Laser intensity	$9.2 \times 10^{20}$	$\text{W}/\text{cm}^2$
$a_0$	20.75	

## LASER-PLASMA SIMULATIONS

### 2D Simulations

The particle-in-cell (PIC) code Smilei [10] was used to simulate the TNSA interaction. A two-dimensional (2D) simulation was performed with a laser defined using the parameters in Table 1 and incident on a thin plastic foil at  $45^\circ$ . An oblique angle is chosen in order to enhance electron heating effects [11]. The simulation took place in a box with dimensions:  $80 \mu\text{m} \times 60 \mu\text{m}$ , with an individual cell size of:  $5 \text{ nm} \times 10 \text{ nm}$ , with each species represented by 128 particles per cell. The proton macroparticles that emerge from the rear of the foil were tracked for 1 ps.

Two plots of the proton macroparticles at the final timestep of 1 ps of the 2D simulation are presented in Fig. 2. From the colours in the plot (corresponding to the kinetic energy), a large spread of proton energies can be seen. The particles are primarily accelerated in the longitudinal  $z$  direction, and largely consist of low energy protons. If one focuses on the higher energy protons, it can be seen that these particles emerge both off-axis ( $\bar{x} \neq 0$ ) and at an angle ( $\bar{p}_x \neq 0$ ). This arises due to the angle of incidence of the laser.

2D simulations suffer from several issues which include producing an enhanced energy spectrum. This arises due to a difference in the electron heating which results in a weaker sheath field in three-dimensions (3D). This is a well-known phenomenon and various energy scaling laws can be applied [12–15]. In order to properly track a beam one would require a 3D particle distribution. Even though some parameters can be relaxed when going from 2D to 3D, the simulations are still computationally expensive.

### Sampling Method

Methods to run a full 3D simulation are being looked into, but in the meantime, a compromise was made to approximate a 3D particle distribution from the 2D results. This was based on the assumption that the kinematic distribution in the newly added  $y$ -axis would be similar to those simulated for the  $x$ -axis. Hence, the same correlations would exist with the longitudinal axis ( $z$ ), momentum, and energy.

First, despite the multidimensional effect leading to an enhanced energy, the energy was left unchanged. The main reason was to preserve the correlation between energy and position from the simulation. Another reason the energy

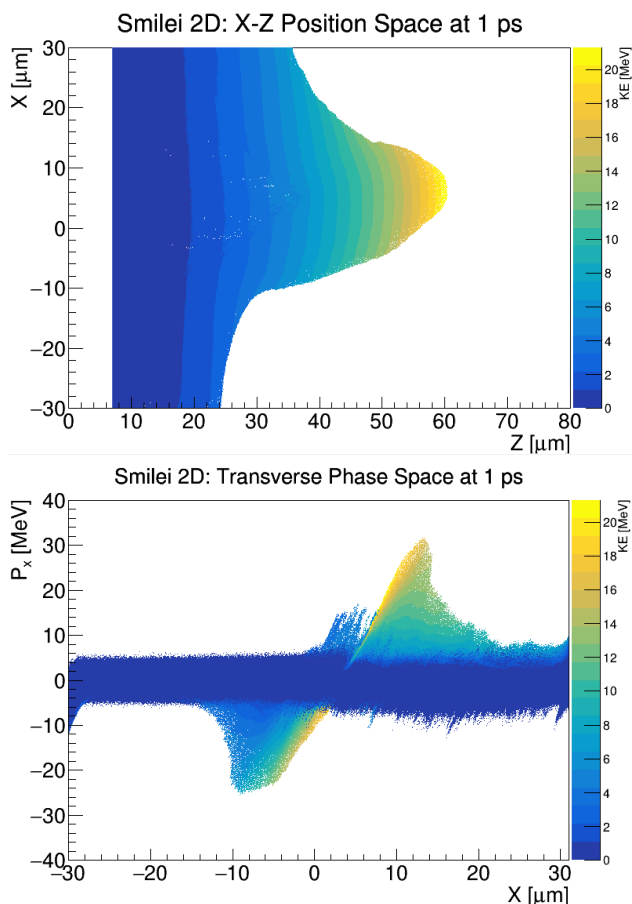


Figure 2: Proton macroparticle plots after 1 ps of the position (top) and transverse phase space (bottom). Colours in both plots correspond to the kinetic energy.

was not scaled was due to a lack of experimental results to compare against. This would lead to an uncertainty in the scaling factor to apply. Even though some scaling factors are given in [12–15], the factors can vary depending on the setup. Furthermore, scaling the energy necessitates a scaling for both momentum and position. Bearing in mind that divergence is a 3D effect [16], it would not necessarily provide a better approximation. Hence, it was decided that it would be more representative of the simulation if the energy was left unchanged. This implicitly assumes a valid approximation could be found for the energies of interest.

Once the energy was sampled, the total momentum of the particle was calculated. To generate the momentum components, two variables were introduced:

$$\theta_p \equiv \arctan\left(\frac{p_x}{p_z}\right), \quad (1)$$

$$\phi_p \equiv \arctan\left(\frac{p_y}{p_z}\right). \quad (2)$$

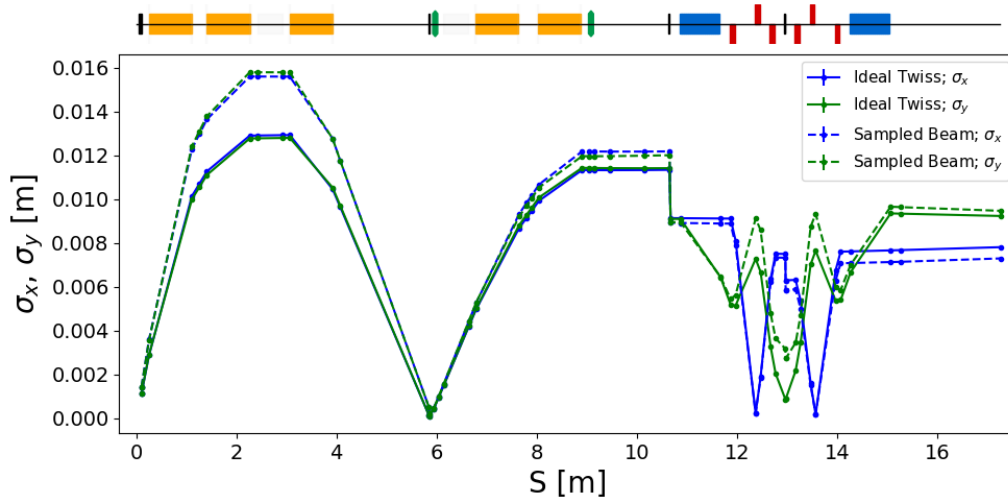


Figure 3: Transverse dimensions of an idealised 15 MeV Gaussian proton beam (solid lines, simulated with an initial bunch of  $\sim 10^4$  particles) and a sampled beam (dashed lines, simulated with an initial bunch of  $\sim 3 \times 10^4$  particles) as a function of position in the Stage 1 beamline. A schematic of the beamline elements is above the plot representative of Fig. 1.

Using these relations and the total momentum,  $p$ , the momentum components could be calculated using:

$$p_z = \sqrt{\frac{p^2}{\tan^2(\theta_p) + \tan^2(\phi_p) + 1}}, \quad (3)$$

$$p_x = p_z \tan(\theta_p), \quad (4)$$

$$p_y = p_z \tan(\phi_p). \quad (5)$$

The position was sampled based on the correlations with the other coordinates. A simple method using 3D histograms was used. The longitudinal position was sampled from a 3D histogram relating the longitudinal position ( $z$ ), longitudinal component of momentum ( $p_z$ ), and the transverse momentum ( $p_x$  and  $p_y$ ). The transverse momentum selected was randomly chosen such that the correlation between the two transverse momentum components and the position was preserved. The transverse positions ( $x, y$ ) were sampled separately from histograms relating the position ( $x, y$ ), the respective transverse components of momentum ( $p_x, p_y$ ), and the longitudinal position ( $z$ ). Finally, the beam was centred for the energies of interest so that it would travel down the centre of the beampipe.

## BEAMLINE TRACKING RESULTS

The Stage 1 beamline was designed for an idealised Gaussian beam specified in [1, 2]. To analyse the performance of the sampled beam, both it and the idealised beam were tracked. The evolution of the beam sizes,  $\sigma_x, \sigma_y$ , are presented in Fig. 3. Both beams were tracked for 5 cm from the target in BDSIM [17], where the presence of electrons suppresses space-charge effects. The beams were then tracked for a further 5 cm in GPT [18] (representing the vacuum nozzle) to include space-charge effects. Space-charge was modelled using the `spacecharge3Dmesh` routine with MGCG Poisson solver method for a fixed-sized mesh of 50, 50,

and 150 mesh lines for the  $x, y$ , and  $z$  directions respectively. A radial cut-off was applied (with a radius of 2.87 mm) to represent the exit aperture of the nozzle. Finally, the beams were tracked through the rest of the beamline in BDSIM using Geant4's QGSP\_BIC\_EMZ physics list. Space-charge was not included for the rest of the beamline because past simulations [1, 2] show only a minor discrepancy in the performance of the beam. For these simulations, the Gabor lenses were simulated with equivalent strength solenoids.

From Fig. 3, it can be seen that although there is an initial discrepancy where the sampled beam grows to a larger beam size, after passing through the collimator (represented by the black box) located at around 6 m, the beam sizes become comparable farther down the beamline. Further analysis of the performance of the sampled beam is ongoing, such as incorporating field maps to model Gabor lenses. Even though the sampled beam only provides qualitative results, these preliminary results give confidence in the design of the beamline, and improves upon past simulations which only involved idealised beams.

## CONCLUSION

Laser-plasma interactions have been simulated for a laser driven proton source. From the 2D laser source simulations, a technique was developed to generate an approximate 3D particle distribution. This sampled beam was tracked and compared against an ideal beam where comparable beam size evolution was found. These results represent a stepping stone, improving upon past simulations. Analysis and optimisations are ongoing to further improve the simulations and tracking.

## REFERENCES

- [1] G. Aymar *et al.*, "LhARA: The laser-hybrid accelerator for radiobiological applications", *Frontiers in Physics*, vol. 8,

- p. 432, 2020.  
doi:10.3389/fphy.2020.567738
- [2] G. Aymar *et al.*, “The laser-hybrid accelerator for radiobiological applications”, 2020. arXiv: 2006.00493.
- [3] S. D. Kraft *et al.*, “Dose-dependent biological damage of tumour cells by laser-accelerated proton beams”, *New Journal of Physics*, vol. 12, no. 8, p. 085 003, Aug. 2010.  
doi:10.1088/1367-2630/12/8/085003
- [4] D. Doria *et al.*, “Biological effectiveness on live cells of laser driven protons at dose rates exceeding 109 gy/s”, *AIP Advances*, vol. 2, no. 1, p. 011 209, 2012.  
doi:10.1063/1.3699063
- [5] K. Zeil *et al.*, “Dose-controlled irradiation of cancer cells with laser-accelerated proton pulses”, *Applied Physics B*, vol. 110, no. 4, pp. 437–444, 2013.  
doi:10.1007/s00340-012-5275-3
- [6] E. L. Clark *et al.*, “Measurements of energetic proton transport through magnetized plasma from intense laser interactions with solids”, *Phys. Rev. Lett.*, vol. 84, pp. 670–673, Jan. 2000.  
doi:10.1103/PhysRevLett.84.670
- [7] A. Maksimchuk, S. Gu, K. Flippo, D. Umstadter, and V. Y. Bychenkov, “Forward ion acceleration in thin films driven by a high-intensity laser”, *Phys. Rev. Lett.*, vol. 84, pp. 4108–4111, May 2000.  
doi:10.1103/PhysRevLett.84.4108
- [8] R. A. Snavely *et al.*, “Intense high-energy proton beams from petawatt-laser irradiation of solids”, *Phys. Rev. Lett.*, vol. 85, pp. 2945–2948, Oct. 2000.  
doi:10.1103/PhysRevLett.85.2945
- [9] S. C. Wilks *et al.*, “Energetic proton generation in ultra-intense laser–solid interactions”, *Physics of Plasmas*, vol. 8, no. 2, pp. 542–549, 2001.  
doi:10.1063/1.1333697
- [10] J. Derouillat *et al.*, “Smilei : A collaborative, open-source, multi-purpose particle-in-cell code for plasma simulation”, *Computer Physics Communications*, vol. 222, pp. 351–373, 2018.  
doi:10.1016/j.cpc.2017.09.024
- [11] Y. Ping *et al.*, “Absorption of short laser pulses on solid targets in the ultrarelativistic regime”, *Phys. Rev. Lett.*, vol. 100, p. 085 004, Feb. 2008.  
doi:10.1103/PhysRevLett.100.085004
- [12] K. D. Xiao *et al.*, “Multidimensional effects on proton acceleration using high-power intense laser pulses”, *Physics of Plasmas*, vol. 25, no. 2, p. 023 103, 2018.  
doi:10.1063/1.5003619
- [13] J. Babaei *et al.*, “Rise time of proton cut-off energy in 2d and 3d pic simulations”, *Physics of Plasmas*, vol. 24, no. 4, p. 043 106, 2017.  
doi:10.1063/1.4979901
- [14] S. Sinigardi, J. Babaei, and G. Turchetti, “Tnsa proton maximum energy laws for 2d and 3d pic simulations”, *Nuclear Instruments and Methods in Physics Research Section A: Accelerators, Spectrometers, Detectors and Associated Equipment*, vol. 909, pp. 438–440, 2018.  
doi:10.1016/j.nima.2018.01.057
- [15] A. Sgattoni, P. Londrillo, A. Macchi, and M. Passoni, “Laser ion acceleration using a solid target coupled with a low-density layer”, *Phys. Rev. E*, vol. 85, p. 036 405, Mar. 2012.  
doi:10.1103/PhysRevE.85.036405
- [16] M. Afshari, J. Hornung, A. Kleinschmidt, P. Neumayer, D. Bertini, and V. Bagnoud, “Proton acceleration via the tnsa mechanism using a smoothed laser focus”, *AIP Advances*, vol. 10, no. 3, p. 035 023, 2020.  
doi:10.1063/1.5117236
- [17] L. J. Nevay *et al.*, “BDSIM: An accelerator tracking code with particle-matter interactions”, *Computer Physics Communications*, vol. 252, p. 107 200, 2020.  
doi:10.1016/j.cpc.2020.107200
- [18] S. B. van der Geer and M. J. de Loos, “Applications of the general particle tracer code”, in *Proc. 17th Particle Accelerator Conf. (PAC’97)*, Vancouver, Canada, May 1997, paper 8P090, pp. 2577–2579.